

Phase Separation of Nonionic Surfactant Aqueous Solution in Standing Surface Acoustic Wave for Submicron Particle Manipulation

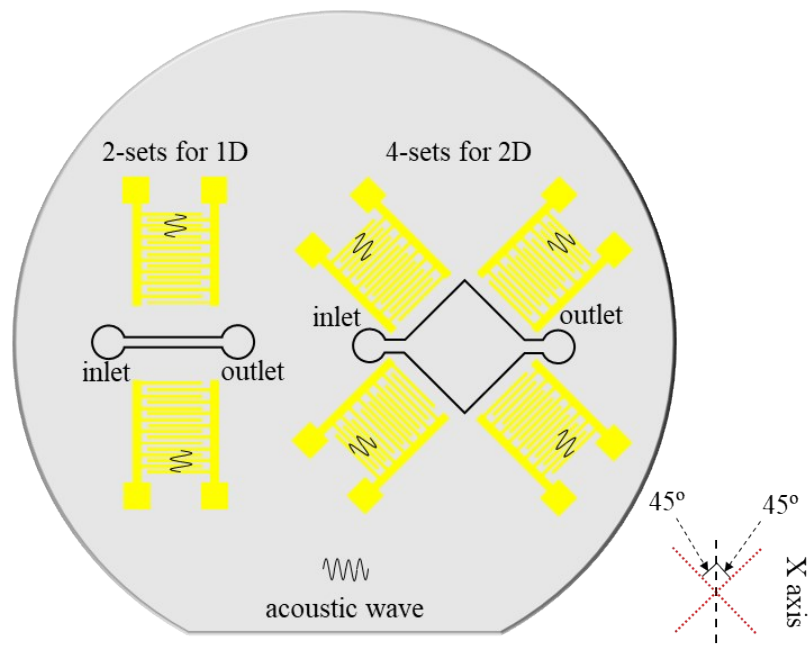
Lei Zhao^{1a}, Pengfei Niu^{1a*}, Eudald Casals², Muling Zeng², Chen Wu¹, Yang Yang¹,
Sheng Sun¹, Zongwei Zheng¹, Zhaoxun Wang¹, Yuan Ning¹, Xuexin Duan¹, Wei
Pang^{1*}

1. State Key Laboratory of Precision Measuring Technology & Instruments, Tianjin
University, Tianjin 300072, China

2. School of Biotechnology and Health Sciences, Wuyi University, Jiangmen,
Guangdong 529020, China

* Corresponding authors: niupengfei2018@tju.edu.cn and weipang@tju.edu.cn

a. These two authors contribute equally



128°Y cut X-Propagation lithium niobate substrate

Figure S1. The schematic drawing of our employed acoustofluidic devices.

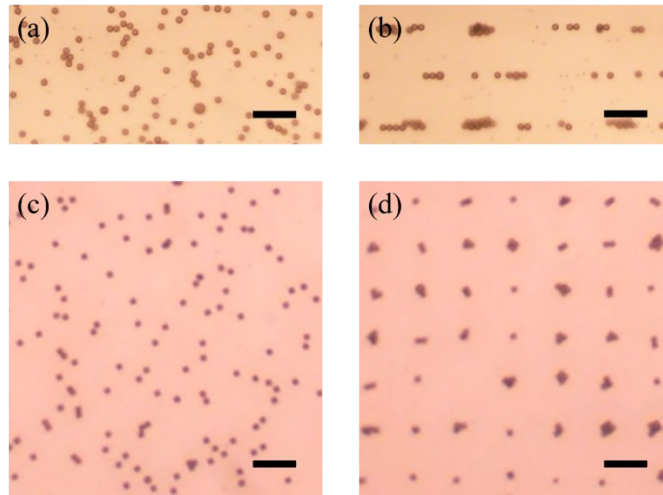


Figure S2. The patterning appearance of 10 μm PS beads in the 1x PBS solution by SSAW field with the wavelength of 150 μm . (a, c) are the captured pictures of the dispersed particles in the microchannel or chamber. (b, d) are the patterns of 10 μm PS particles obtained by two sets and four sets of transducers respectively, frequencies of which are 25.5 MHz and 27.6/27.7 MHz, respectively. The scale bar for the captured Figures is 75 μm .

Table S1. The correlation of critical micelle concentration and temperature of Tween 20 in water¹

Temperature (°C)	25	40	55	65	75
CMC (mM)	0.0499	0.0342	0.0149	0.0161	0.0171

The separation out of Tween 20 from water results in two separated phases: one contains much of the surfactant, generally named as surfactant-rich phase, while the other has largely water with surfactant concentration around its critical micelle concentration (CMC). Wherein CMC is the surfactant concentration at and above which micelles are formed.

Table S1 reprints the published results of the CMC of Tween 20 in water at increased temperatures¹. At each of these listed temperatures, there will be micelle formation (i.e., phase separation and making the liquid to be inhomogeneous) when the Tween 20 surfactant concentration is above the corresponding CMC value listed in the Table S1. Maybe the phase separation just above this critical point is very hard to visually observe, but it exists.

Table S2. The concentration of our added Tween 20 surfactant in 1x PBS solution

Volume Concentration (v/v)	2%	5%	10%
Molar Concentration (mM)	0.018	0.045	0.09

Table S2 lists the molar concentration of our added Tween 20 surfactant in 1x PBS solution. The used molecular weight of Tween 20 surfactant is 1228g/mol. The critical temperatures which can cause the micelle formation (i.e., phase separation) of our used 1x solution with Tween 20 volume concentration of 2% and 5% are ~50°C and ~30°C, respectively. So, if the liquid temperature in the microchannel or chamber is higher than ~50°C and ~30°C, phase separation can occur. With respect to the solution containing 10% (v/v) Tween 20, surfactant micelles already form under our operated temperature conditions due to the high concentrations even without the SSAW being on.

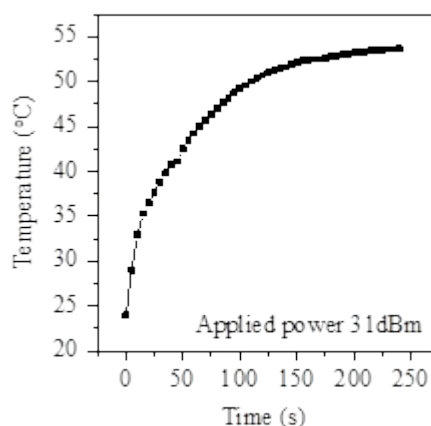
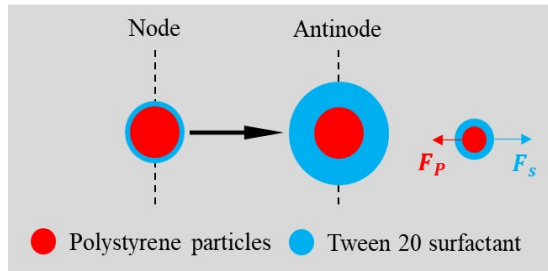


Figure S3. The increase of temperature with time from 0 to 4 min of 1x PBS solution in the microchannel recorded by an infrared thermometer under the applied power of 31dBm in our system. This applied power is the same as those used for our particle patterning experiments. The used acoustofluidic platform contains two sets (one pair) transducers. And the time scale is a little bit shorter than our experiments.

Figure S3 plots the increase of temperature with time from 0 to 4 min of 1x PBS solution in the microchannel or chamber recorded by an infrared thermometer under the applied power of 31dBm in our system. It goes up to around 30°C and 50°C after around few seconds and 2 minutes after two transducers are on. We placed a cooling platform underneath, so the temperature does not increase continuously, and reach a plateau at around 55°C. So, this rise in temperature for sure can induce the micelle formation and phase separation of Tween 20 in our system.

It is worthy to note that this temperature increase occurs just with one pair of transducers. We believe the temperature increase will be stronger and faster if two pairs are on together. and phase separation can occur easier in two pairs system.



- ❑ Extra accumulation of Tween 20 surfactant on the polystyrene particles during phase separation;
- ❑ Force (F_p) to the polystyrene particle part to node direction;
- ❑ Force (F_s) to the surfactant part towards antinode direction.

Figure S4. Our proposed mechanism for the location migration of particles from pressure nodes to antinodes.

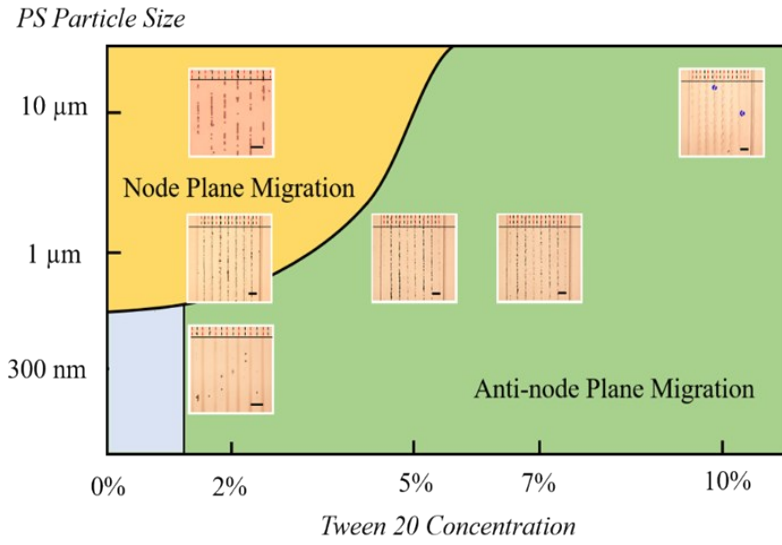


Figure S5. The variation of patterned locations of different sized polystyrene particles at solutions with various surfactant concentrations. Our employed platform has one pair of transducers. The acoustic wavelength is $150\mu\text{m}$. and the applied power is 31 dBm.

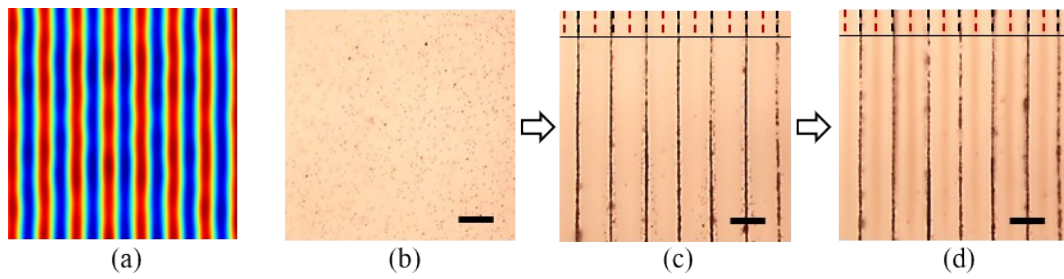


Figure S6. The patterning appearance of 300 nm and 1 μm PS particles in 2% (v/v) Tween 20 1x PBS solution by SSAW field with the wavelength of 150 μm . (a) is the simulated acoustic pressure distribution of device with two sets of transducers. Colors from blue to red represents the minimum to maximum values. Three key patterned moments are captured, i.e. (b) the initial state, (c) the 1 μm /300nm beads being patterned at pressure nodes (PN) and (d) 300 nm beads are migrated to antinodes (PAN), respectively. PNs and PANs are marked by black and red dashed lines. The scale bar for the captured Figure is 75 μm .

Table S3. Parameters of aqueous solution with 2% and 10% (v/v) Tween 20 surfactant at 20°C

Material	Symbol	Value
2% Tween 20 aqueous solution		
Density	ρ_m	1000 kg·m ⁻³
Sound velocity	c_m	1487 m·s ⁻¹
Shear viscosity	μ	1.2 mPa·s
Bulk viscosity	μ_b	3.5 mPa·s
Compressibility	κ_m	452 TPa ⁻¹
10% Tween 20 aqueous solution		
Density	ρ_m	1001 kg·m ⁻³
Sound velocity	c_m	1505 m·s ⁻¹
Shear viscosity	μ	1.65 mPa·s
Bulk viscosity	μ_b	4.8 mPa·s
Compressibility	κ_m	441 TPa ⁻¹

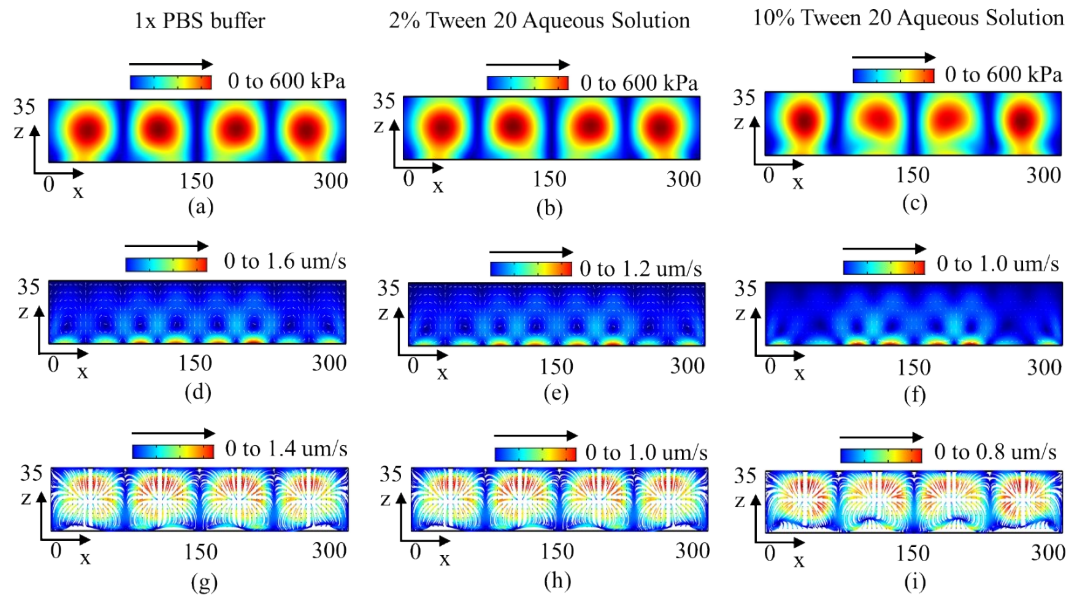


Figure S7. The comparison results of acoustic pressure (a) (b) (c), acoustic streaming effect (d) (e) (f) and the trajectories of 3 μm PS beads (g) (h) (i), 1x PBS solution (a) (d) (g) and solution with 2% Tween 20 (b) (e) (h), and 10% Tween 20 (c) (f) (i) under the displacement amplitude of LiNbO₃ piezoelectric substrate.

The addition of tween 20 increase the viscosity and the compressibility (derivative of bulk modulus) of the 1x PBS liquid. Table S3 lists these parameters for liquids with 2% and 10% Tween content respectively. Assuming no phase separation occurs, we studied the impact of Tween 20 content on the produced acoustic pressure, acoustic streaming as well as the trajectories of 3 μm PS beads in pure 1x PBS media or those with surfactants under the displacement amplitude of LiNbO₃ piezoelectric substrate.

As can be seen from Figure S7 (a), (b) and (c), the acoustic pressure horizontal distribution of these three liquids is almost same, while in the vertical direction, the position of the pressure node/anti-node distribution shows a slight difference due to the different sound velocity in these liquids. Acoustic streaming results (Figure S7(d), (e) and (f)) demonstrate that the liquid streaming velocity declines with the rise of surfactant content. Moreover, 3 μm PS particles mainly expose to acoustic radiation force in all of these studied liquids, and they can be accumulated at the pressure node locations with reduced movement velocity when the surfactant content is high. Therefore, higher content of surfactant just suppresses the particle movement velocity (Figure S7(g), (h) and (i)) but has nearly no impact on the accumulation outputs. Our simulation results are consistent with existing publication⁵.

Glycerol and 1x PBS are miscible and no phase separation occurs. Adding glycerol increases the liquid's viscosity and bulk modulus. We carried out the 300 nm polystyrene particle patterning experiment in PBS liquid with glycerol, the particles cannot be accumulated and regularly patterned. So, we believe the change in viscosity and compressibility of liquid with the Tween 20 surfactant presence is not the cause for submicron particle patterning and the location migration. Phase separation should be associated with the phenomenon observed in this work.

1. Simulation of acoustophoresis driving by standing surface acoustic waves

a) Governing equations

Governing equations for a linear viscous compressible fluid are the continuity and the Navier–Stokes equations which are the mass and momentum balance laws, respectively. In addition, an equation of state between p and ρ is assumed. In the equations, p , ρ , v , μ_b , μ and c_0 are the fluid pressure, mass density, fluid velocity, bulk viscosity, shear viscosity and sound velocity in the fluid at rest.

$$\frac{\partial \rho}{\partial t} + \nabla \cdot (\rho v) = 0 \quad (1)$$

$$\rho \frac{\partial v}{\partial t} + \rho (v \cdot \nabla) v = -\nabla p + \mu \nabla^2 v + \left(\mu_b + \frac{1}{3}\mu\right) \nabla(\nabla \cdot v) \quad (2)$$

$$p = c_0^2 \rho \quad (3)$$

These three equations determine the viscous compressible fluid system but with nonlinear effects to solve the acoustic radiation force (ARF) and acoustic streaming force (ASF) which are the main forces driving the movement of particles in this system. To consider these nonlinear effects, we employ Nyborg's perturbation approximation which takes first and second order (subscript 1 and 2) of basic variables into account:

$$\rho = \rho_0 + \rho_1 + \rho_2 \quad (4)$$

$$p = p_0 + p_1 + p_2 \quad (5)$$

$$v = v_1 + v_2 \quad (6)$$

Substituting the perturbation approximation into governing equations and the state equation, then setting the sum of all the terms of order two in a non-dimensional small parameter (defined as the ratio between the amplitude of the boundary excitation and a characteristic length) to zero and finally averaging the resulting equations over a period of oscillation, we gain the time-averaged second-order continuity equation and Navier–Stokes equation:

$$\rho_0 \nabla \cdot \langle v_2 \rangle = -\nabla \cdot \langle \rho_1 v_1 \rangle \quad (7)$$

$$\rho_0 \left\langle \frac{\partial v_2}{\partial t} \right\rangle + \left\langle \rho_1 \frac{\partial v_1}{\partial t} \right\rangle + \rho_0 \langle v_1 \cdot \nabla v_1 \rangle = -\nabla \langle p_2 \rangle + \mu \nabla^2 \langle v_2 \rangle + \left(\mu_b + \frac{1}{3}\mu\right) \nabla(\nabla \cdot \langle v_2 \rangle) \quad (8)$$

It should be noted that the angled brackets $\langle \dots \rangle$ denote a time average over an oscillation period and when $A(t)$ and $B(t)$ complex-valued variables with harmonic time-dependence $e^{i\omega t}$, there is

real-part rule $\langle A(t)B(t) \rangle = \frac{1}{2} \text{Re}[A(0)^* B(0)]$, in which the asterisk represents complex conjugation.

b) Boundary conditions

A two-dimension standing surface acoustic wave microfluidic model was built with height being 35 μm and width being 300 μm which was twice the wavelength. The lower boundary simulated interface velocity actuated by SSAW which takes form¹:

$$v_x = \zeta d_0 \omega \left[e^{-C_d \left(\frac{W}{2} - x\right)} e^{i \left[-k \left(\frac{W}{2} - x\right)\right]} + e^{-C_d \left(\frac{W}{2} + x\right)} e^{i \left[k \left(\frac{W}{2} - x\right)\right]} \right] \quad (9)$$

$$v_y = -d_0 \omega \left[e^{-C_d \left(\frac{W}{2} - x\right)} e^{i \left[-k \left(\frac{W}{2} - x\right) - \theta\right]} - e^{-C_d \left(\frac{W}{2} + x\right)} e^{i \left[k \left(\frac{W}{2} - x\right) - \theta\right]} \right] \quad (10)$$

where $v_x, v_y, \zeta, d_0, C_d, W, \theta$ is interface velocity in x direction and y direction, displacement amplitude proportion, y-component displacement amplitude of the SAW, SAW attenuation coefficient, channel width and phase difference. The other boundary simulating PDMS microchannel walls applied a lossy-wall condition which takes form:

$$n \cdot \nabla p = i \frac{\omega \rho_m}{\rho_{PDMS} c_{PDMS}} p \quad (11)$$

where $p, \rho_m, \rho_{PDMS}, c_{PDMS}$ is first-order acoustic pressure, density of medium, PDMS density and sound velocity.

c) Particle acoustophoretic trajectory affected by ARF and ASF

For a spherical particle suspended in fluid surrounding SSAWs, the acoustic radiation force (ARF) and acoustic streaming force (ASF) are the main forces driving the movement of particles in this system. After obtaining the acoustic fields p and u from the 2D model, by adopting the theory of Gor'kov, the time-averaged radiation force potential, which is also called Gor'kov potential (U_{rad}), the ARF (F_{rad}) on the spherical particle suspended in fluid can be determined through:

$$f_1 = 1 - \frac{\kappa_p}{\kappa_m}, f_2 = \frac{2[1 - \Gamma](\rho_p - \rho_m)}{2\rho_p + \rho_m - 3\Gamma} \quad (12)$$

$$\Gamma = -\frac{3}{2} [1 + i(1 + \delta)] \delta, \delta = \frac{\delta}{a} \quad (13)$$

$$U_{rad} = \left[\frac{f_1}{4\kappa_m} \text{Re}(p_1 \cdot p_1^*) - \frac{3\rho_m f_2}{8} \text{Re}(v_1 \cdot v_1^*) \right] \pi a^3 \quad (14)$$

$$F_{rad} = -\partial_z U_{rad} \quad (15)$$

In these expressions, a , ρ_p κ_p are the radius, density and compressibility of a compressible, spherical particle, ρ_m and κ_m are density and compressibility of an inviscid fluid, δ is the viscous penetration depth which is defined 0.1 μm for ultrasound waves at 26 MHz in water.

The ASF on a spherical particle is given by simple formula:

$$F_{drag} = 6\pi\mu a(\langle v_2 \rangle - v_p) \quad (16)$$

where v_p is velocity of the particle and $\langle v_2 \rangle$ is obtained from 2D modelling numerical simulation.

For steady flows, we can identify the bead trajectories with the streamlines of the velocity field.

Table S4. Parameters used in the numerical simulations

Parameter	Symbol	Value
Water		
Density	ρ_m	997 kg·m ⁻³
Sound velocity	c_m	1497 m·s ⁻¹
Shear viscosity	μ	0.89 mPa·s
Bulk viscosity	μ_b	2.47 mPa·s
Compressibility	κ_m	448 TPa ⁻¹
1x PBS		
Density	ρ_m	1003.8 kg·m ⁻³
Sound velocity	c_m	1631 m·s ⁻¹
Shear viscosity	μ	0.904 mPa·s
Bulk viscosity	μ_b	2.5 mPa·s
Compressibility	κ_m	374.5 TPa ⁻¹
Polystyrene		
Density	ρ_{PS}	1050 kg·m ⁻³
Compressibility	κ_{PS}	259 TPa ⁻¹
Tween 20 ²		
Density	$\rho_{Tween20}$	1070 kg·m ⁻³
Compressibility	$\kappa_{Tween20}$	457 TPa ⁻¹
PDMS (10:1)		
Density	ρ_{PDMS}	920 kg·m ⁻³
Sound velocity	c_{PDMS}	1076 m·s ⁻¹
LiNbO ₃		
Sound velocity	c_{LN}	3994 m s ⁻¹
Else		
Wavelength	λ	150 μm
Frequency	ω	26.6 MHz
Width	W	300 μm
Height	H	35 μm
Displacement amplitude	d_0	1 nm
Displacement amplitude proportion	ζ	0.86
Displacement decay coefficient ³	C_d	116 m ⁻¹
Phase difference	θ	$\pi/2$

2. Calculation of acoustic contrast factor

In theory, the particle's patterning location depends on its acoustic contrast factor, which is derived from the acoustic radiation force that dominates to acoustophoretic particle patterning behaviour. The two sets oppositely placed SSAW field can be simplified as two series of planar waves propagating in opposite directions and encountering in space. Considering the aforementioned 1D planar standing wave, along the z-axis it can be described by the expression 17:

$$p(z) = p_a \cos(kz), \text{ with } k = \frac{\omega}{c} \quad (17)$$

where k is the wavenumber which is equal to the angular frequency ω divided by sound velocity c . p_a is the pressure field amplitude. Assuming a compressible, spherical particle in an ultrasound planar standing wave field, it will experience an acoustic radiation force F_{rad} as being a weak point-scatterer of acoustic waves through first-order scattering theory. The force can be described by the following equations 18-21:

$$U_{rad} = \left[\frac{f_1 \cos^2(kz)}{3} - \frac{f_2 \sin^2(kz)}{2} \right] \pi a^3 \kappa_m p_a^2 \quad (18)$$

$$F_{rad} = -\partial_z U_{rad} = 4\pi \Phi_{ac} a^3 E_{ac} \sin(2kz) \quad (19)$$

$$f_1 = 1 - \frac{\kappa_p}{\kappa_m}, f_2 = \frac{5\rho_p - 2\rho_m}{2\rho_p + \rho_m} \quad (20)$$

$$\Phi_{ac} = \frac{f_1}{3} + \frac{f_2}{2} = \frac{1}{3} \left[\frac{5\rho_p - 2\rho_m}{2\rho_p + \rho_m} - \frac{\kappa_p}{\kappa_m} \right] \quad (21)$$

where U_{rad} is the Gor'kov potential, E_{ac} is the acoustic energy density and Φ_{ac} is the acoustic contrast factor. The discussional particle needs to be small enough ($a \ll \lambda$). Acoustic contrast factor Φ_{ac} is an important factor which determines the direction of acoustic radiation force F_{rad} acting on the particle. When it is positive, acoustic radiation force drives the particle to the PN locations where the Gor'kov potential is the minimum for it. On the contrary, when it is negative, acoustic radiation force drives the particle to the PAN where the Gor'kov potential is the minimum for it. Acoustic contrast factor Φ_{ac} is decided by the differences of particle's density and compressibility from fluid media. Table S2 lists the density and compressibility of polystyrene beads, Tween 20, and 1x PBS.

Table S5. Parameters used in calculation of acoustic contrast factor

	Density	Compressibility
1x PBS	1003.8 kg·m ⁻³	374.5 TPa ⁻¹
Polystyrene	1050 kg·m ⁻³	259 TPa ⁻¹
Tween 20	1070 kg·m ⁻³	457 TPa ⁻¹

Video S1. The numerical simulation of 500 nm PS particles in a SSAW field.

Video S2. The experimental process of 10 µm and 300 nm PS particle patterning in the one pair of transducers generated SSAW field, the applied frequency being 25.5 MHz.

Video S3. The experimental process of 10 µm and 300 nm PS particle patterning in the two pairs of transducers generated SSAW field, the applied frequency being 27.6/27.7 MHz.

Video S4. The experimental process of 1 µm and 300 nm PS particle patterning in the one pair of transducers generated SSAW field, the applied frequency being 25.5 MHz.

Video S5. The clouding and patterning behavior of Tween 20 with the concentration of 10% (v/v).

References

1. May Essa Mahmood et al., *Global Journal of Science Frontier Research Chemistry*, 2013, 13(4), 1-7.
2. D. Köster, *SIAM Journal on Scientific Computing*, 2007, **29**, 2352-2380.
3. F. M. Sannaningannavar, S. N. Patil, R. M. Melavanki, B. S. Navati and N. H. Ayachit, *Journal of Molecular Liquids*, 2014, **196**, 244-248.
4. N. Nama, R. Barnkob, Z. Mao, C. J. Kähler, F. Costanzo and T. J. Huang, *Lab on a Chip*, 2015, **15**, 2700-2709.
5. Peter Barkholt Muller et al. A numerical study of microparticle acoustophoresis driven by acoustic radiation forces and streaming-induced drag forces, *Lab on a Chip*, 2012,12, 4617-4627.